Center for Advanced Materials

CAM

Presented at the 1988 TMS Annual Meeting, Phoenix, AZ, January 25–28, 1988, and to be published in the Proceedings

Exploratory Development in the System Al-Sc-X

R.R. Sawtell and J.W. Morris, Jr.

January 1988

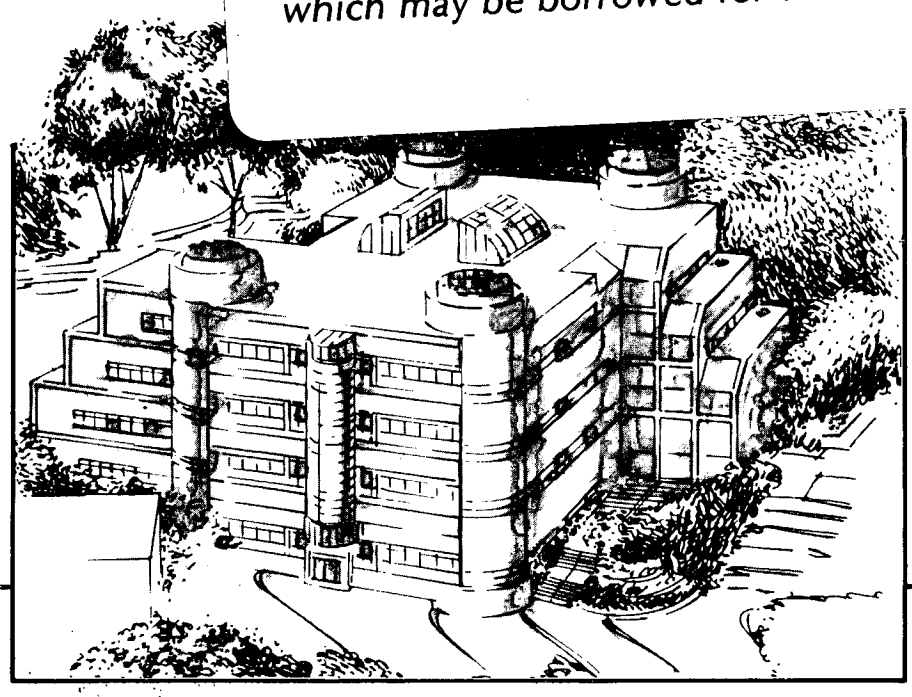

Materials and Chemical Sciences Division

Lawrence Berkeley Laboratory • University of California

ONE CYCLOTRON ROAD, BERKELEY, CA 94720 • (415) 486-4755

Prepared for the U.S. Department of Energy under Contract DE-AC03-76SF00098

DISCLAIMER

LBL 24626

Exploratory Development in The System Al-Sc-X

Ralph R. Sawtell and J. W. Morris, Jr.

Center for Advanced Materials
Materials and Chemical Sciences Division
Lawrence Berkeley Laboratory
University of California
and
Department of Materials Science and Mineral Engineering
University of California at Berkeley
Berkeley, California 94720

January 1988

This work is jointly supported by the Director, Office of Energy Research, Office of Basic Energy Science, Materials Sciences Division of the U. S. Department of Energy under Control No. DE-AC03-76SF00098 and the Aluminum Company of America

Exploratory Development in the System Al-Sc-X

Ralph R. Sawtell and J. W. Morris, Jr.

Center for Advanced Materials, Lawrence Berkeley Laboratory, and
Department of Materials Science and Mineral Engineering
University of California, Berkeley, California 94720

In the search for new structural materials, systems based on the cubic, Al_3X phase show particular promise both as monolithic materials and as dispersions in an Al matrix. One of the most interesting candidates is the Al_3Sc phase which has been observed as a highly stable, coherent precipitate in Al alloys. Al-Sc-X alloys hardened by this phase have been shown to develop unique combinations of properties. This work examines the Al(ss)→ Al_3Sc phase transition for the purpose of predicting potential substitutes or replacements for Sc. Theoretical analyses of intermetallic compound formation and precipitation in the Al-Sc-RE (RE=rare earth elements) are described as are the results of experimental evaluations of such systems. These results include descriptions of new Al-Sc-RE alloys with tensile strengths as high as 310MPa (45 ksi); some of the highest levels attained in an Al alloy on a per atom basis.

I. Introduction

Although the unique properties of Al alloys containing scandium have been known for many years [1], this system has received relatively little attention because of the cost and scarcity of Sc. In Al-base alloys Sc combines with Al to form a stable precipitate that has the stoichiometric composition Al_3Sc and an ordered, $L1_2$ structure. The phase precipitates as very small coherent, spherical particles [2]. Because of the low solubility of Sc in Al the achievable precipitate volume fraction is small. Nonetheless Sc additions contribute significantly to alloy strength; in fact, Sc is the most potent strengthener known for Al based systems [1,3-5]. The Al_3Sc precipitate is also extremely effective in stabilizing the substructure of Al alloys, and hence facilitates the use of strain hardening and stabilization treatments to further augment strength. The combined effects of precipitation and strain hardening have been used to produce tensile strengths in the range of 250 MPa in Al-Sc alloys. While these strength levels are too low to be of commercial interest for structural alloys, the addition of ternary solid solution strengtheners raises the strength to competitive levels. Al-Sc-Mg alloys have been produced with very attractive combinations of density, strength, fracture toughness and corrosion resistance [6].

The exceptional thermal stability of the Al_3Sc precipitate may also prove useful in alloy design. For many years, researchers have sought methods to improve the dismal elevated temperature performance of high performance Al alloys. Recent work [7,8] has emphasized dispersion hardening because of the inherently high coarsening rates of the common hardening precipitate phases. While promising dispersion-hardened alloys have been developed, their usefulness is compromised by the need for powder processing to fabricate usable products, by the relatively high density caused by the heavy alloy elements used, and by low fracture toughness, which is due, in part, to the incoherent nature of the

dispersions. Because the Al_3Sc precipitate is coherent and unusually resistant to coarsening there is good reason to expect that Al-Sc alloys can be designed to retain high strength and fracture toughness at elevated temperature.

Despite the promise of Al-Sc alloys, their potential is limited by the cost and limited availability of Sc. A possible solution to this problem is to substitute alloying additions that are similar in nature to Sc to reduce the Sc content without sacrificing properties. If viable substitutes exist they may also enhance the properties of Al-Sc-(X) alloys, either by increasing the attainable precipitate fraction or improving the hardening efficiency of the precipitate phase. The quest for such substitutes is the subject of this research. Both the scientific rationale for candidate alloying choices and results of initial experimental work will be presented.

II. Theory

While a search for Sc substitutes may be done in a purely empirical way, the length of the periodic table suggests the use of metallurgical theory to identify promising species. The theoretical challenge is to predict which elements or combinations of elements interact synergistically with Sc to produce similar distributions of coherent precipitates. This requires considering at least three different phenomena: (1) the formation of intermetallic compounds that resemble Al_3Sc, (2) the precipitation of such compounds from solid solution in Al, and (3) the influence of the precipitates on alloy strength. Fortunately, these subjects have been well studied.

A. Intermetallic Compounds

The obvious first step in a search for elements that behave like Sc is to consider the other elements that share its grouping in the periodic table. Scandium, a group IIIA element, should be similar to Y and the Lanthanide or rare earth elements (RE). Unfortunately, very little detailed information exists on the phases formed by even binary combinations of Al and rare earth elements. Still less is available for ternary combinations. Given the lack of experimental data we rely on the available simple theories of intermetallic formation. These are based on two key considerations: chemical interactions, which can often be associated with differences in electronegativity, and elastic interactions, which are due to difference in atom size. Table I presents the metallic radii and electronegativities of the group IIIA elements.

Table I: Radii and Electronegativity for Various Elements

Element	Atomic Number	Ionic Radius (nm)	Metallic Radius (nm)	Electronegativity
Al	13	0.057	0.143	1.61
Sc	21	0.0730	0.162	1.36
Y	39	0.0905	0.1802	1.22
Ce	58	0.1034	0.182	1.12
Pr	59	0.1013	0.182	1.13
Nd	60	0.0995	0.182	1.14
Sm	62	0.0964	0.182	1.17
Gd	64	0.0938	0.1801	1.20
Tb	65	0.0923	0.1782	1.20
Dy	66	0.090	0.1773	1.22
Ho	67	0.0894	0.1765	1.23
Er	68	0.0881	0.1757	1.24
Tm	69	0.0869	0.1720	1.25
Yb	70	0.0858	0.179	1.10

The electronegativity difference between Al and Sc is small, which suggests that the bonding between the two is predominantly metallic or covalent. Most of the rare earth elements have electronegativity values very similar to Sc, with Y and Gd through Tm being the closest. The comparability of the electronegativity difference suggests that these elements should strongly resemble Sc in their chemical interaction with Al.

In contrast to the electronegativity values, there is a substantial difference between the metallic radii of Al and Sc (12%). The rare earth elements are all significantly larger than Sc. It is hence likely that differences in the behavior of the IIIA alloying additions in Al will be associated with size, or elastic effects. The rare earth elements that are closest to Sc in size are Y and the series Gd through Tm.

There is a reasonable body of experimental information on the intermetallic compounds that form between aluminum and the rare earth elements of interest [9]. A review of this work reveals that the observed intermetallic structures can be divided into three types: (1) Al_3X compounds with, (2) cubic Mg_2Cu-type Laves phases and (3) orthorhombic AlDy-type structures. Consistent with the discussion above, these are all so-called "size factor" compounds. We are primarily interested in the Al-rich phases with Al_3X stoichiometry. This category includes a variety of related crystal structures that are based on different stacking sequences of ordered {111} planes [10-12]. In all cases, the stable structure is the one that minimizes crystal volume; the structure of the binary intermetallic is determined by the size mismatch between Al and the rare earth element in question. The structural trend is shown in Figure 1, in which we have plotted the cube root of the cell volume (a') against the rare earth atom size for all of the binary Al_3X structures. The Cu_3Au-type, $L1_2$ crystal structure, which is typified by Al_3Sc, is favored when the size difference is small or the pressure is high [11]; the smallest rare earth elements

(Er,Tm,Yb) form stable $L1_2$ structures and the next largest (Ho, Tb) can be induced into this structure by raising the external pressure. The upper limit on the rare earth metallic radius for formation of an $L1_2$-type Al_3X structure lies at about 0.176nm at atmospheric pressure and about 0.178nm at high pressure.

The lattice parameters of the $L1_2$-type Al_3X phases differ from those that are predicted from a calculation that uses Vegard's Law and the metallic radii of the elements. Interestingly, however, the error in the calculation is almost constant for all of the compounds of interest and is about 5.5%. Since we do not have reliable data on the Vegard's Law parameter for the solid solution, it is not now known what part of this discrepancy is associated with the effective atom size in the Al matrix and what part is due to additional atomic contraction in the precipitate phase.

The relation between structure and atomic size in the aluminum-rare earth compounds suggests the existence of ternary compounds with the $L1_2$ structure and the stoichiometric formula $Al_3(Sc_{1-x}X_x)$. If chemical effects can be neglected the $L1_2$ structure should be favored for combinations of scandium and rare earth elements that produce an effective size, $r_{eff} = (1-x)r_{Sc}+(x)r_{RE}$, less than about 0.176 nm. We would thus anticipate an inverse relationship between the size of a rare earth element and its maximum solubility in the $L1_2$ structure. A number of such ternary intermetallic compounds have been observed experimentally [13,14]. A representative list is given in Table II which also includes the reported solubility limit, the lattice constant at the solubility limit and the value of the effective radius (r_{eff}) at the solubility limit. When the effective size is considered, these intermetallics follow the same structural trends as the binary trialuminides (Figure 1.). As expected, the maximum reported solubility decreases as the rare earth size increases. However, the reduction is larger than expected; none of these compounds achieves an effective radius near the limit found for the binary intermetallics (0.176 nm). In addition, except for Y which may differ somewhat in its chemistry, the effective radius at maximum solubility decreases with increasing rare earth size. This effect may be a simple consequence of the distortion of the Sc-RE sublattice of the $L1_2$ structure caused by the size difference.

It should also be noted that the reported maximum solubility of Gd in the $L1_2$ form of $Al_3(Sc_xGd_{1-x})$ is well below that which would be expected from the behavior of the binary or the other ternary compounds. We suspect that this is an experimental error. The results given later in the paper suggest a much higher solubility limit.

Table II. Ternary $Al_3(Sc_{1-x}RE_x)$ Intermetallics

Phase	RE Radius (nm)	Maximum Solubility	Lattice* Parameter (nm)	Effective Radius (nm)
$Al_3(Sc_{1-x}Er_x)$	0.1757	0.9	0.4160	0.1745
$Al_3(Sc_{1-x}Ho_x)$	0.1765	0.72	0.4199	0.1730
$Al_3(Sc_{1-x}Dy_x)$	0.1773	0.4	0.4190	0.1720
$Al_3(Sc_{1-x}Tb_x)$	0.1782	0.57	0.4196	0.1701
$Al_3(Sc_{1-x}Gd_x)$	0.1801	0.15	0.4118	0.1664
$Al_3(Sc_{1-x}Y_x)$	0.1802	0.6	0.4168	0.1705

* At the reported maximum x

B. Precipitation

In the previous section we considered the stable intermetallic configurations in the Al-Sc-RE system. To complete the picture we must consider the precipitation of these compounds from solid solution. We are interested in the $L1_2$ structures that may replace Al_3Sc. The thermodynamic driving force for precipitation at given temperature and pressure, ΔG, is

$$\Delta G = V\beta(\Delta g_c + \Delta g_e) + A\beta(\gamma_{\alpha\beta}) \quad (1)$$

where $V\beta$ is the precipitate volume, Δg_c and Δg_e are, respectively, the chemical and elastic free energy changes per unit volume of precipitate phase, $A\beta$ is the interfacial area of the precipitate and $\gamma_{\alpha\beta}$ is the interfacial tension. To phrase a simple model we use the fact that the electronegativities of the species of interest here are nearly the same to neglect the chemical free energy difference between them. If we also neglect differences in interfacial tension, the differences in the driving force for nucleation for the various compositions is determined by differences in the elastic energy.

The change in elastic energy on forming a precipitate (which is equal to the change in the elastic contribution to the free energy) is

$$\Delta g_e = N[e_p - e_s] \quad (2)$$

where N is the number of solute atoms in the precipitate, e_p is the elastic energy of the precipitate per solute atom and e_s is the elastic energy per solute atom in the solution. Assuming linear elasticity, elastic isotropy and homogeneous elastic constants [15], the elastic energy of an inclusion per unit volume is

$$E_e = \left(\frac{2}{9}\right) G \left[\frac{1+\nu}{1-\nu}\right] \varepsilon_0^2 \quad (3)$$

where G and ν are, respectively, the shear modulus and Poisson's ratio of the elastic medium and ε_0 is the stress-free strain of the inclusion. To apply this relation to precipita-

tion from solid solution we require values for the stress-free strain, ε_0, of the precipitate and the solute atom in solution. For the solution,

$$\varepsilon_0 \cong 3(\delta r/r) \tag{4}$$

where r is the radius of and aluminum matrix atom and $\delta r = r_{eff} - r$, where r_{eff} is the effective radius of the precipitate. Strictly, we should compute the effective radius in solution from the Vegard's Law constants of the solute species. Since this data is unavailable, we use the metallic radii of the free atoms. For the precipitate,

$$\varepsilon_0 \cong 3(\delta a/a) \tag{5}$$

where a is the lattice parameter of the FCC unit cell, $\delta a = a' - a$ where a' is the lattice parameter of the $L1_2$ cell of the precipitate, and we have assumed complete precipitation of the available solute. Using these relations

$$\Delta g_e = 2G\left[\frac{1+\nu}{1-\nu}\right]\left\{v_s\left(\frac{da}{a}\right)^2 - \Omega_s\left(\frac{dr}{r}\right)^2\right\} \tag{6}$$

where Δg_e is the free energy change per atom of solute, v_s is the volume of precipitate per atom of solute and Ω_s is the volume per atom in the solid solution. While v_s is four times Ω_s, the solute strain (dr/r) is always much greater than the precipitate strain (da/a), with the consequence that the elastic energy term is always negative and promotes precipitation. The magnitude of the effect increases with the atomic size and atom fraction of the ternary rare earth addition.

These results suggest that so long as the atom fraction of the ternary rare earth addition is low enough that all of it can be incorporated into the $L1_2$ precipitate, its presence should increase both the volume fraction and the thermal stability of the precipitate phase. The ternary addition should, hence, be decidedly beneficial, provided that it does not diminish the strengthening effect of the precipitate phase.

C. Strengthening

The influence of an array of precipitates on alloy strength is determined by its effect on the critical resolved shear stress for dislocation glide [16], which is related to the tensile yield strength by the Taylor factor. The critical resolved shear stress (τ_c) for glide through a random distribution of like obstacles is given by the relation [17]

$$\tau_c = 0.9\left(\frac{2T}{l_s b}\right)\beta_c^{3/2} \tag{7}$$

where T is the line tension of the dislocation, b is its Burgers' vector, l_s is the mean spacing between obstacles, and β_c is the dimensionless "strength" of the obstacle, that is, the maximum effective force with which it resists the passage of a dislocation. A real solid contains a distribution of hardening precipitates, and equation (7) must be modified to

account for the different precipitate sizes and effective radii in the glide plane. A method for doing this is described in reference [18], which shows that the strengthening effect of the precipitate phase can still be related to its maximum effective strength, β_c.

The obstacle strength (β_c) depends on the dominant hardening mechanism [16]. In the case of coherent, $L1_2$ precipitates the dominant hardening mechanism is usually either order hardening, in which case the obstacle strength is proportional to the antiphase boundary energy in the precipitate phase, or elastic hardening, in which case β_c is proportional to the elastic misfit, ε_0. In either case the results of the previous section suggest that the strength of Al_3Sc precipitates should be increased by partial substitution of an atom that is larger, but chemically similar to Sc. The elastic strain induced by the precipitate increases directly with atom size. The antiphase boundary energy is a more subtle property, but, to a first approximation, it increases with the stability of the precipitate phase relative to the disordered solution [19,20], and should, therefore, increase with the difference between the elastic energy of the precipitate and that of the solution.

D. Implications for Alloy Design

The considerations discussed above suggest that the volume fraction, stability and hardening effect of precipitates in an alloy containing a given amount of scandium will be improved by adding a ternary addition of any of the elements listed in Table II. The benefit is expected to increase with the atomic size of the ternary element, provided that it is fully incorporated into the hardening precipitate without changing its $L1_2$ structure. From this perspective the optimal addition will be determined by a balance between the increasing size, which promotes stability and hardening, and decreasing size, which promotes solubility in the $L1_2$ structure.

To test these ideas we added equal amounts of elements selected from the list in Table II to a base Al-Sc alloy. The amount of alloy addition was chosen in the expectation that it would exceed the solubility limit for the larger ternary additions, but not for the smaller ones, and would hence let us study the balance between the size effect on the inherent hardening by the precipitate phase and the inverse effect on solubility in the precipitate phase, which determines the total amount of precipitate that will form. As we shall discuss below, this effort was successful in producing alloys with promising properties. Surprisingly (and encouragingly), we apparently did not exceed the solubility of any of the ternary additions.

III. Materials and Experimental Procedure

In order to evaluate and refine the theory presented in the previous section a series of Al-Sc-(RE) alloys were cast and fabricated. A list of these alloys is shown in Table III. All of the ternary alloys contained 0.3 atom percent of both scandium and the ternary addition, which would produce a hardening precipitate with the stoichiometric formula $Al_3Sc_{0.5}X_{0.5}$ if all of the rare earth were incorporated into the precipitate. The specific

ternary additions were chosen because they cover both the limits of binary $L1_2$ stability and the known $Al_3(Sc_{1-x}X_x)$ structures. The binary Al-Sc alloy was included as a control.

The alloys were melted and cast using standard chill cast techniques. The ingots were cast in rectangular cross section (6.35 x 76.2 x 76.2 mm) Cu molds. The small ingot thickness was useful to ensure mildly rapid solidification rates (10-100K/sec.) and, thus, enhance supersaturation in the as-cast condition. All ingots were trimmed to remove solidification defects. Sections of each ingot were cold swaged to 2.5 mm and then cold drawn into wire samples 0.44 mm in diameter. Subsequent aging and annealing treatments were performed in circulating air furnaces within $\pm$ 1 K of set temperature.

Table III: Chemical Compositions of Al-Sc-(X) Alloys in Weight Percent*

System	Sc	Gd	Y	Ho	Er
A-Sc	0.5				
Al-Sc-Er	0.5				1.8
Al-Sc-Ho	0.5			1.8	
Al-Sc-Y	0.5		1.0		
Al-Sc-Gd	0.5	1.7			

*Weight fractions were chosen to yield 0.3 atom percent of both Sc and X

Tensile properties were measured by adhesively bonding the wire samples to gripping blocks and straining at a constant rate of 1.66×10^{-4} per second. Because of the low loads involved, a small, digitally controlled load frame was developed and used for the tests. Due to the small sample size, the strain could not be measured reliably. Only the tensile strength is reported here; however, since there was negligible work hardening, the tensile and yield strengths are essentially the same.

The alloy microstructures were studied with optical and transmission electron microscopy, using a Philips 301 electron microscope for the latter. Electrical resistivity was determined using a 4-point probe and a standard Kelvin bridge at a temperature of 293$\pm$1K. Differential scanning calorimetry (DSC) was used to clarify the solubility limit of Sc in Al and monitor solid state precipitation reactions. A Perkin Elmer DSC-7 was used for this purpose.

IV. Results and Discussion

A. Phase Relationships

Although little phase diagram information is available for Al-RE alloys, the Al-Sc phase diagram has been investigated and offers some insight into optimum fabrication schemes. The Al end of the Al-Sc binary phase diagram, as originally determined by Willey [21], is shown in Figure 2. More recent work by Fujikawa et. al. [22], based on resistivity, agrees well with the solid solubility data presented in this figure but is in some con-

flict on the eutectic temperature. DSC analysis of the material used in this study yielded a value of 931.8K, which is in good agreement with Willey's data.

As shown in Figure 2, the system is characterized by an extremely shallow α+liquid phase field and, thus, a very narrow freezing range. It is, therefore, relatively easy to obtain a supersaturated solid solution from the melt for binary alloys with up to about 0.52 weight percent Sc, the composition at which primary Al_3Sc begins to form. This scandium content is considerably above that which could be incorporated with a solution annealing treatment, since the maximum solid solubility of Sc is about 0.38. Hence, no attempts were made to solution heat treat these alloys.

B. DSC Results

The formation enthalpy for the $L1_2$ phase was determined for each alloy by measuring the heat of precipitation during continuous heating at a rate of 20K/min. The measured values of ΔH_{ppt} recorded for the binary Al-Sc control, as well as the ternary Al-Sc-RE alloys, are shown in Table IV.

Table IV: ΔH_{ppt} Values for Al-Sc-(X) Alloys

Alloy	ΔH_{ppt}* (J/g)	Metallic Radius† (nm)
Al-Sc	2.22	0.162
Al-Sc-Er	2.41	0.1757
Al-Sc-Ho	2.61	0.1765
Al-Sc-Y	2.90	0.1802
Al-Sc-Gd	2.97	0.1801

* At heating rate of 20K/min..
† For Sc or RE.

If the ternary additions were not present in solid solution or did not participate in the precipitation reaction, the values of ΔH_{ppt} for the ternary alloys would be identical to those for the binary Al-Sc alloy. However, the ΔH_{ppt} values for the ternaries are all greater than for the binary, which indicates that the ternary species participate. The ternary addition might affect the results in either of three ways: by increasing the total amount of precipitate, by changing the nature of the precipitate, or by increasing the stability of the precipitate. Given that ΔH_{ppt} increases with solute atom size, and that (as discussed below) no additional precipitates are observed, it is most likely that the change in ΔH_{ppt} reflects the increase in precipitate stability that is anticipated from the theory of the previous section.

Despite the changes in ΔH_{ppt}, there were no changes in precipitation kinetics or activation energy as determined by examining peak shifts as a function of the DSC scan rate.

C. Artificial Aging Behavior

To further study the differences between the alloys, both tensile strength and electrical resistivity were measured as a function of aging temperature and time. The aging temperature was varied from 508 to 583K. Normal aging behavior was noted in all alloys, typified by an initial rapid increase in strength to a peak value followed by softening. Peak strength was obtained with approximatly 10 hours of aging at 558K. The electrical resistivity monotonically decreased with increasing temperature or time. For any given alloy, electrical resistivity is uniquely determined by the precipitate type and size and, thus, can be used to normalize the aging temperature. This means that aging data for several aging temperatures can be plotted on a single curve. The measured tensile strengths of the alloys are plotted against the electrical resistivity in Figure 3. Third order polynomial regression curves are also plotted to make the trends more clear. The peak strength for each alloy and the resistivity at peak strength are presented in Table V. Excepting the Al-Sc-Er alloy, both the peak tensile strength and the resistivity at peak strength increase with solute atom size, a behavior which tracks that found for ΔH_{ppt}.

Table V: Peak Tensile Strength and Resistivity at Peak Strength for Al-Sc-(X) Alloys

Alloy	Peak Strength (MPa)	Resistivity (μ ohm-cm)	Metallic Radius (nm)
Al-Sc	251	3.033	0.162
Al-Sc-Er	278	3.094	0.1757
Al-Sc-Ho	262	3.073	0.1765
Al-Sc-Y	290	3.080	0.1802
Al-Sc-Gd	309	3.128	0.1801

D. Microstructure

Transmission electron microscopic studies of the alloys in the peak aged condition revealed that each contained only one discernible precipitate phase, which had the $L1_2$ crystal structure of Al_3Sc. The substructures of the ternary alloys were likewise similar to one another and to the Al-Sc binary, consisting of an extremely fine distribution of irregular subgrains. Even in the peak aged condition the precipitates in this system are too small to allow a reliable determination of precipitate composition with the facilities available to us. However, the incorporation of rare earth elements should change the precipitate lattice constants to an observable degree. Additional high resolution TEM studies are in progress.

E. Discussion

When these experimental observations are combined with the theoretical analysis of the previous section a self consistent picture seems to emerge. First, since only one type of precipitate is observed to account for the change in properties associated with the ternary additions, it is very likely that the ternary additions have been incorporated into the $L1_2$

phase to produce precipitates of the type $Al_3(Sc_{1-x}X_x)$. The monotonic increases in strength and stability with increasing rare earth size strongly suggests that essentially all of the rare earth component is contained in the precipitates. This result is surprising since the prior work reviewed above suggests that the larger rare earth species have relatively low solubility in Al_3Sc. The apparent presence of precipitate phases with high (x=0.5) substitutions of the larger rare earth elements may reflect inaccuracies in the accepted solubility limits for these species, or it may result from non-equilibrium effects, such as metastable precipitation in the presence of a high thermodynamic driving force and a strong lattice constraint. In any case, the trends in both strength and ΔH_{ppt} are consistent with the predictions of the theoretical model.

The variation of resistivity at peak strength with peak strength is also consistent with the model. It is well known that resistivity increases with decreasing particle size in the range of interest here. Thus, our results indicate that peak strength occurs at smaller precipitate sizes as the radius of the ternary solute increases. Research on the microstructural determinants of peak strength in alloys that are hardened by coherent precipitates [18] shows that the strength maximum occurs when the precipitates have coarsened to the extent that the largest of them are just large enough to be looped by dislocations (the Orowan mechanism) rather than cut by them. Since the larger ternary additions should produce precipitate particles with greater resistance to the passage of dislocations (greater strength, β_c), these species should also produce strength maxima at smaller particle sizes, hence higher electrical resistance.

The initial results of this work are of technological as well as scientific interest. The experimental data indicates that the maximum tensile strength of an Al-0.5Sc-1.8Gd alloy is 310 MPa, which is 25 percent higher than the largest strength obtained with binary Al-Sc alloys. This is a very promising result and makes this class of alloys the highest strength I/M Al alloys on a per atom basis. Given the preliminary nature of the work, substantial further improvements are almost certainly possible. It is likely that ternary rare earth additions will prove very useful in the design of aluminum alloys with exceptional structural properties.

Acknowledgments

This work was jointly supported by the Aluminum Company of America and by the Director, Office of Energy Research, Office of Basic Energy Science, Material Sciences Division of the U. S. Department of Energy under control No. DE-AC03-76SF00098. The authors are grateful to Shelley Miyasato, Center for Advanced Materials, LBL, for assistance in the TEM work, and to A.G. Khachaturyan and Judith Glazer, Center for Advanced Materials, LBL, for helpful discussions.

References

1. L. A. Willey, *U.S. Patent 3,619,181*, 1971.

2. M. E. Drits, S. G. Pavlenko, L. S. Toropova, Yu. G Bykov and L. B. Ber, *Sov. Phys. Dokl.*, 1981, vol. 26, pp 344-346.

3. M. E. Drits, L. S. Toropova and Yu. G. Bykov, *Metallovedenie. i Termicheskaya. Obbrabotka. Metallov*, 1983, vol. 7, pp 60-63.

4. V. I. Elagin, V. V. Zakharov and T. D. Rostova, *Metallovedenie. i Termicheskaya. Obbrabotka. Metallov*, 1983, vol. 7, pp 57-60.

5. N. Blake and M. A. Hopkins, *J. Mat. Sci.*,1985, vol. 20, pp 2861-67.

6. R. R. Sawtell, *U.S. Patent 4,689,090*, 1987.

7. G. J. Hildeman and R. E. Sanders, *U. S. Patent 4,379,719*, 1983.

8. S. L. Langenbeck, J. M. Cox, G. J. Hildeman, D. K. Denzer, R. J. Rioja, C. W.Cho and J. W Simon, *Elevated Temperature Al Alloy Development*, AFWAL Contract F33615-81-C-5096, March 1984.

9. A. Iandelli and A. Palenzona, *Handbook on the Physics and Chemistry of Rare Earths*, Ed. Gschneidner and Eyring, North Holland, 1979.

10. J. H. Van Vucht and K. H. J. Buschow, *J. Less-Common Metals*, 1965, vol. 10, pp 98-107.

11. J. F. Cannon and H. T. Hall, *J. Less-Common Metals*, 1975, vol. 40, pp 313-328.

12. M. Gasgnier, G. Schiffmacher and P. Caro, *J. Less-Common Metals*, 1976, vol. 50, pp 177-188.

13. O. I. Zalutskaya, V. G. Kontsevoy, N. I. Karamyshev, V. R. Ryabov and I. I. Zalutsky, *Dop. Akad. Nauk. Ukrain. RSR [A]*, 1970, vol. 8, pp 751-753.

14. O. I. Zalutskaya, V. R. Ryabov and I. I. Zalutsky, *Dop. Akad. Nauk. Ukrain. RSR [A]*, 1970, vol. 3, pp 255-259.

15. A. G. Khachaturyan, *Theory of Structural Transformations in Solids*, John Wiley & Sons, 1983.

16. A. J. Ardell, *Metall. Trans. A*, 1985, vol. 16A, pp 2131-2165.

17. K. Hanson and J. W. Morris, *J. Appl. Phys.*, 1975, vol. 46, pp 983-990.

18. J. Glazer and J. W. Morris, *Acta Met.*, 1988, In press.

19. P. A. Flynn, *Trans. AIME*, 1960, vol. 218, pp145-154.

20. A. G. Khachaturyan and J. W. Morris, *Phil. Mag.*, 1987, vol. 56, pp517-532.

21. L. A. Willey, *Alcoa Laboratories Physical Metallurgy Division Report 13-62-EH3*, 1962.

22. S. I. Fujikawa, M. Sugaya, H. Takei and K. I. Hirano, *J. Less Common Metals*, 1979, vol. 63, pp 87-97.

Figure Captions

Figure 1. Plot of the cube root of unit cell volume (a') against the rare earth ionic radius for various Al_3RE intermetallics. Note the trend toward the Cu_3Au-type, $L1_2$ crystal structure for smaller metallic radii.

Figure 2. The Al-Sc phase diagram as determined by Willey. Note the extremely shallow Al+L phase field.

Figure 3. Plot of tensile strength versus resistivity for a number of Al-Sc-(RE) alloys aged at temperature between 508 and 583K. Note the trend towards higher peak strength for alloys containing larger RE.

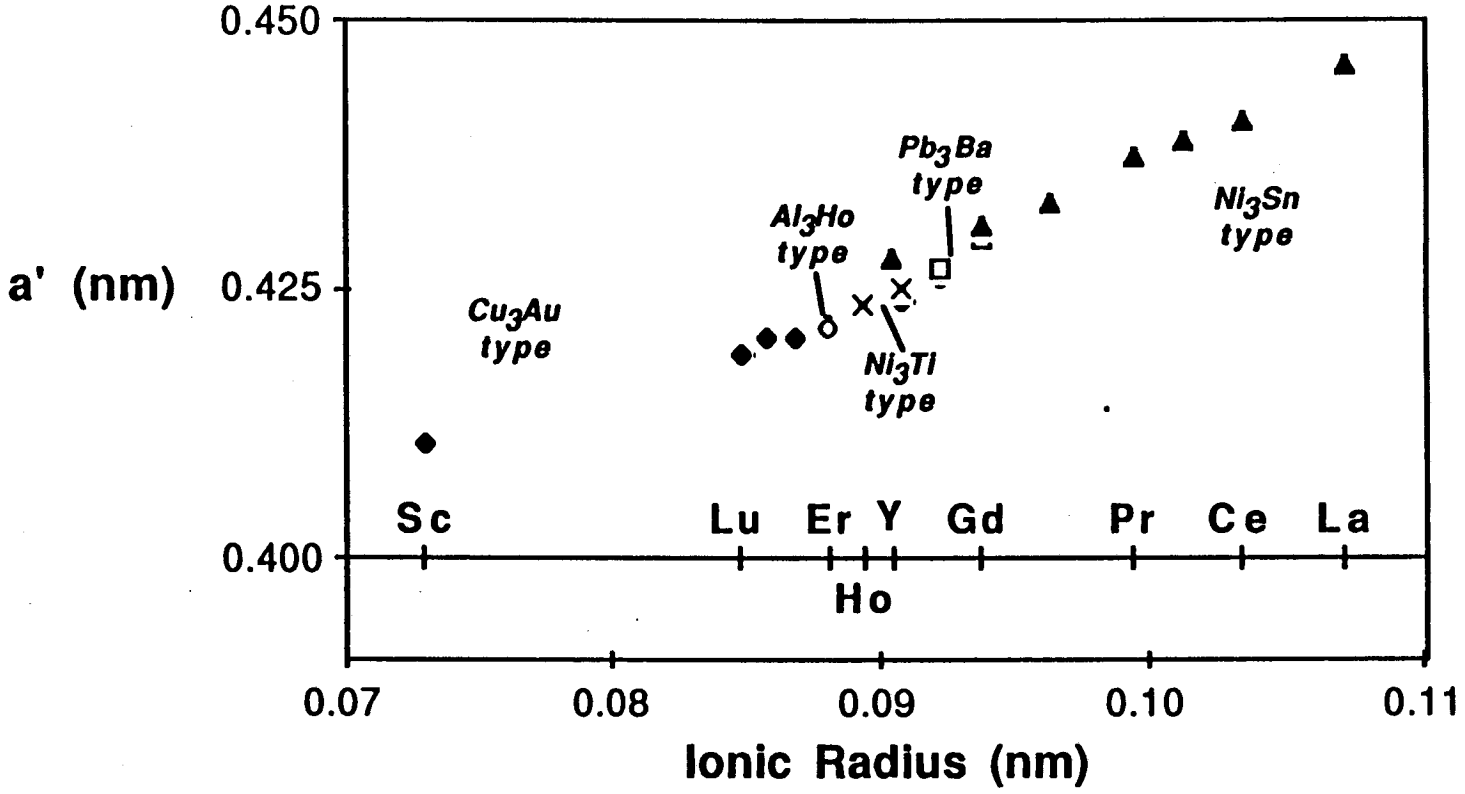
0.450
0.425
0.400
a' (nm)
Cu3Au type
Al3Ho type
Pb3Ba type
Ni3Tl type
Ni3Sn type
Sc
Lu
Er
Y
Gd
Pr
Ce
La
Ho
0.07
0.08
0.09
0.10
0.11
Ionic Radius (nm)
XBL 882-593

Figure 1.

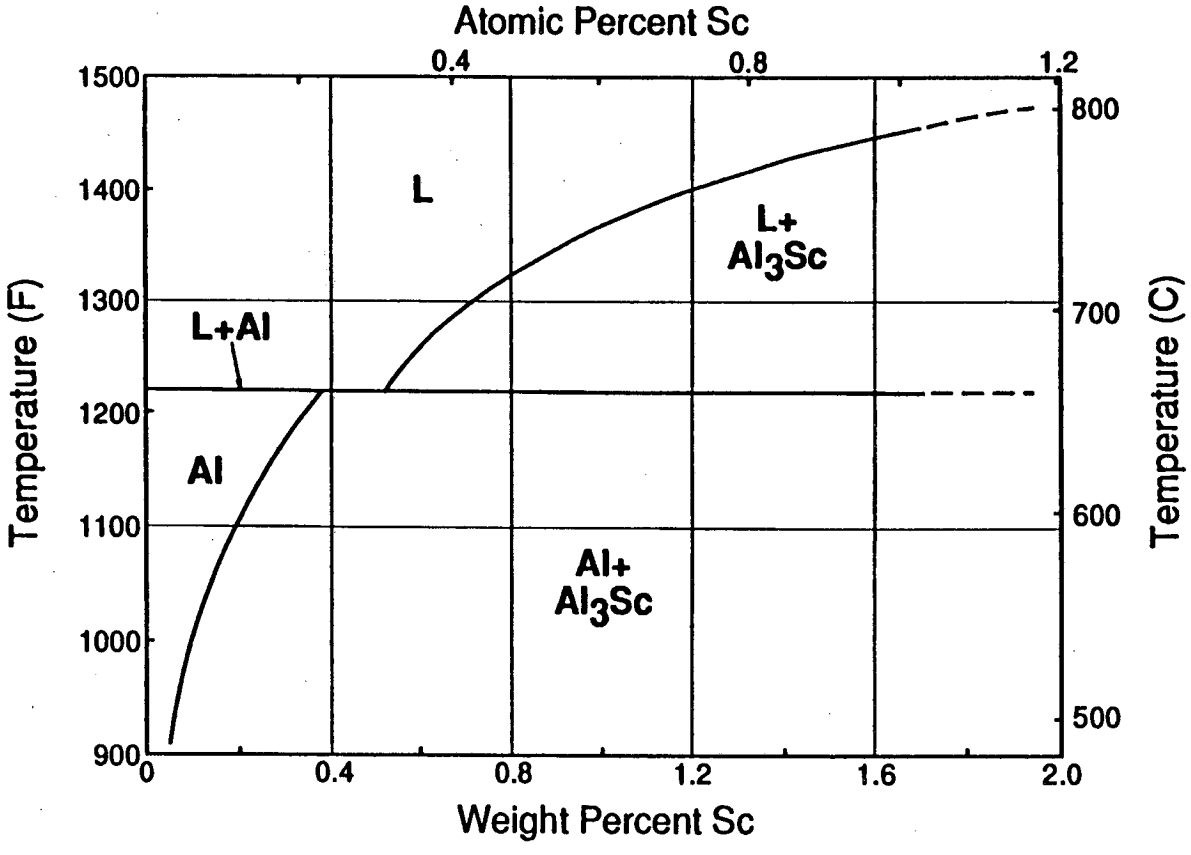

Figure 2. Al-rich section of the Al-Sc phase diagram.

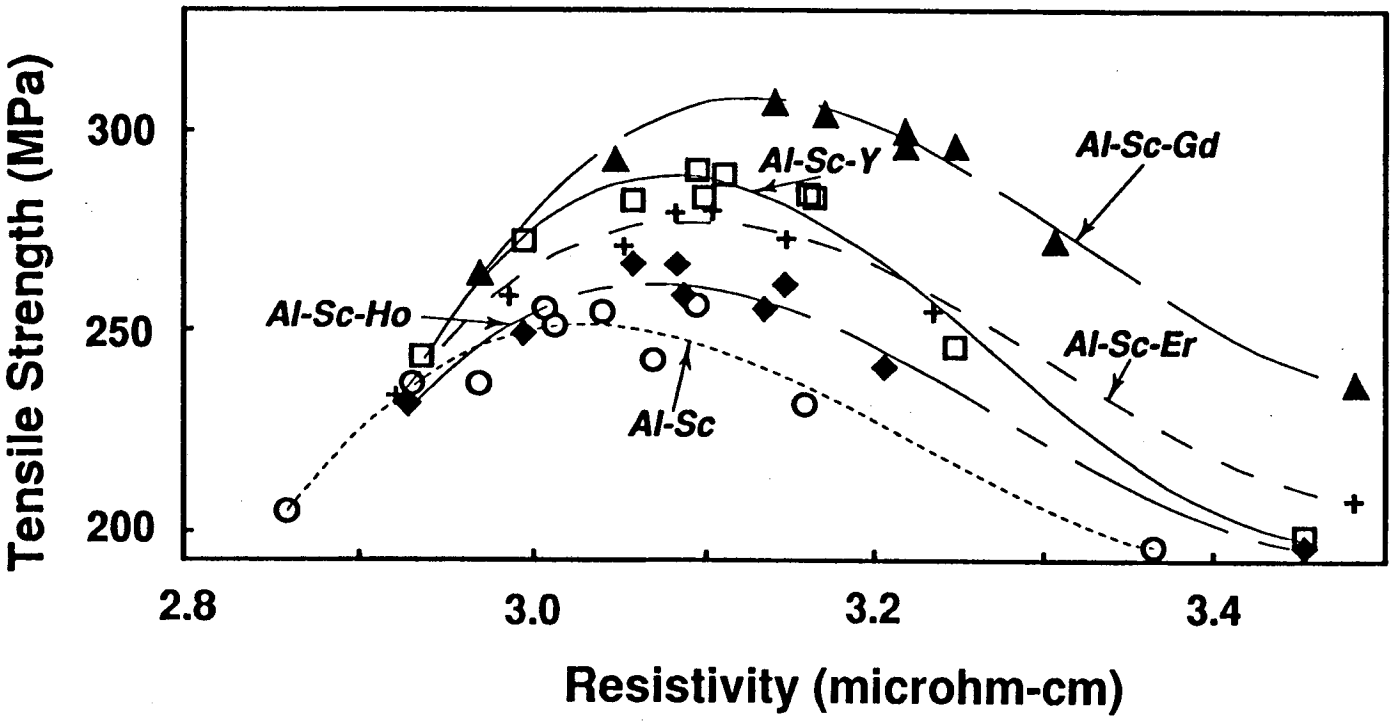

- XBL 882-591 -

Figure 3

LAWRENCE BERKELEY LABORATORY
TECHNICAL INFORMATION DEPARTMENT
UNIVERSITY OF CALIFORNIA
BERKELEY, CALIFORNIA 94720